We are IntechOpen,
the world's leading publisher of
Open Access books
Built by scientists, for scientists

4,800
Open access books available

122,000
International authors and editors

135M
Downloads

154
Countries delivered to

Our authors are among the

TOP 1%
most cited scientists

12.2%
Contributors from top 500 universities

BOOK CITATION INDEX
CLARIVATE ANALYTICS
INDEXED

WEB OF SCIENCE™

Selection of our books indexed in the Book Citation Index
in Web of Science™ Core Collection (BKCI)

Interested in publishing with us?
Contact book.department@intechopen.com

Numbers displayed above are based on latest data collected.
For more information visit www.intechopen.com

Methods for Postprocessing in Single-Step Diffuse Optical Tomography

Alexander B. Konovalov[1], Vitaly V. Vlasov[1], Dmitry V. Mogilenskikh[1],
Olga V. Kravtsenyuk[2] and Vladimir V. Lyubimov[2]
[1]Russian Federal Nuclear Center – Zababakhin Institute of Applied Physics, Snezhinsk
[2]Institute for Laser Physics of Vavilov State Optical Institute Corporation, St.Petersburg
Russia

1. Introduction

The methods of computed tomography – X-ray computed tomography, magnetic resonance imaging, single-photon emission computed tomography, positron emission tomography, ultrasonic reflectivity tomography and others (Webb, 1998) are now widely used in the practice of medical imaging and their importance increasingly grows. These methods allow the real time reproduction and visual analysis of the inner spatial structure of tissue on the display, which on whole helps increase the quality of diagnostics. However, in the context of problems to be resolved in oncology, the efficiency of currently available commercial tomography methods remains relatively low. One of the reasons is the lack of methods that would allow reliable differentiation between malignant and benign tumors on reconstructed tomograms. The recent clinical studies (Boas et al., 2001; Gibson et al., 2005) show that rapidly developing diffuse optical tomography (DOT) is very likely to help out. DOT is unique in its ability to separately reconstruct the spatial distributions of optical parameters (absorption and scattering coefficients) which helps visualize the spatial pattern of blood volume and oxygen saturation. As a result, it becomes possible to differentiate and spatially localize such phenomena as cancerous tissue vascularisation and angiogenesis and hence detect cancer in the early stage of its development.

DOT implies that tissue is probed by near-infrared radiation from the so-called therapeutic window (700-900 nm) where absorption by tissue is minimal. Position dependent measurements are taken, i.e. near-infrared light from an array of sources is observed with an array of receivers. Then an inverse problem, i.e. the tomographic reconstruction problem is solved to infer the spatially localized optical properties of tissue. The main problem of DOT is the low spatial resolution because of the multiple scattering of photons that do not have regular trajectories and are distributed in the entire volume V being probed. As a result, each volume element significantly contributes to the detected signal. The basic equation of DOT is written as

$$g(\mathbf{r}_s,\mathbf{r}_d) = \int_V f(\mathbf{r})W(\mathbf{r},\mathbf{r}_s,\mathbf{r}_d)d^3r, \qquad (1)$$

where $g(\mathbf{r}_s, \mathbf{r}_d)$ is the optical projection measured for source position $\mathbf{r}_s$ and receiver position $\mathbf{r}_d$ (usually the relative signal disturbance due to optical inhomogeneities), $f(\mathbf{r})$ is the sought function of optical inhomogeneity distribution (later on the object function), and $W(\mathbf{r}, \mathbf{r}_s, \mathbf{r}_d)$ is a weight function which provides for the contribution of each volume element to the signal formed between the points $\mathbf{r}_s$ and $\mathbf{r}_d$. Equation (1) and hence the inverse problem of DOT are strongly nonlinear because of the nonlinear dependence of photon flux on optical parameters. The local linearization of the inverse problem is performed, as a rule, by using multistep reconstruction algorithms (Arridge, 1999; Yodh & Chance, 1995) based on the variational formulation of the equation that describes the radiation transport model. A classical example of these algorithms is the Newton-Raphson algorithm with the Levenberg-Marquardt iterative procedure (Arridge, 1999). The multistep algorithms allow gaining relatively high spatial resolution (0.3~0.5 cm) for diffusion tomograms, but they are not as fast as required for real time diagnostics. The reason is that the forward problem of DOT, i.e. the problem of radiation propagation through tissue is solved numerically many times and at each step of linearization it is necessary to adjust the matrix of the system of algebraic equations that describe the discrete reconstruction model.

As shown in our earlier papers (Kalintsev et al., 2005; Konovalov et al., 2003; 2006b; 2007a; 2007b; Lyubimov et al., 2002; 2003), there exists a unique opportunity to make the reconstruction procedure much faster by changing over in equation (1) from volume integration to integration along an effective trajectory from source to receiver. The photon average trajectory method (PAT method) we have developed finds such a trajectory using a probabilistic interpretation of light energy transfer by photons from source to receiver. The method introduces the density of the conditional probability $P[\mathbf{r}, \tau \,| \,(\mathbf{r}_s, 0) \rightarrow (\mathbf{r}_d, t)]$ that a photon migrating from a space-time source point $(\mathbf{r}_s, 0)$ to a space-time receiver point $(\mathbf{r}_d, t)$ reaches a point $\mathbf{r} \in V$ at time τ $(0 \le \tau \le t)$. The effective trajectory is a photon average trajectory (PAT) described by the mass center of the spatial distribution P over a time t. If we deal with absorbing inhomogeneities, then in the approximation of perturbation theory by Born or Rytov, integral (1) can be written as the fundamental equation of the PAT method (Kravtsenyuk & Lyubimov, 2000; Lyubimov et al., 2002; 2003)

$$g(\mathbf{r}_s, \mathbf{r}_d, t) = \int_L v(l) \left\{ \int_V f(\mathbf{r}) P[\mathbf{r}, \tau \,| \,(\mathbf{r}_s, 0) \rightarrow (\mathbf{r}_d, t)] d^3 r \right\} dl, \qquad (2)$$

where L is the PAT from the source point $\mathbf{r}_s$ to the receiver point $\mathbf{r}_d$, l is distance along the PAT, and $v(l)$ is a factor meaning the inverse relative velocity of the mass center of the distribution P along the PAT. The volume integral in the braces is the sought object function $f(\mathbf{r})$ averaged over the spatial distribution of the photons that contribute to the signal recorded at time t. If denote the averaging operator by $<\cdot>$, we can write (2) in a more compact form as

$$g = \int_L v(l) < f(\mathbf{r}) > dl. \qquad (3)$$

Equation (3) is an analog of the Radon transform and can be inverted for the function $< f(\mathbf{r}) >$ with the fast algorithms of projection tomography.

It is well known (Kak & Slanay, 1988; Herman, 1980) that there are two different approaches to the solution of type (3) integral equations. The first is based on their analytical solution

and the use of the resulted inversion formulas for finding the object function in discrete points of space. The second consists in the representation of the integral equation as a system of linear algebraic equations which is solved for the set of unknowns that define the discrete values of the object function. Replacing volume integral (1) by trajectory integral (3) in both the approaches makes it possible to change over from multistep to single-step reconstruction. For the first approach this means that the integral formulas for inverting equation (3) are linear and no linearization steps are needed. For the second approach the single-step reconstruction means that the system of algebraic equations describing the discrete model is only once inverted and the matrix needs no adjustment.

In our previous papers we provided some examples of 2D reconstruction from data simulated for the time-domain measurement technique to show that the PAT method can be implemented with integral algorithms (Konovalov et al., 2003; 2007b; Lyubimov et al., 2003) as well as with algebraic ones (Konovalov et al., 2006b; 2007a; Lyubimov et al., 2002). Compared with the multistep algorithms, the former give a terrific gain (a factor of about 100) in calculation time, but are too inaccurate in the reconstruction of optical inhomogeneities near the boundaries of the study object. This is since the implementation of the integral inversion formulas has to be done through a linear (or rough piecewise-linear) approximation of PATs that really bend near boundaries because of avalanche photon migration outside the object. The algebraic algorithms are not so fast, but successfully treat the bended trajectories partly compensating for this shortcoming. However on the whole one must admit that the integral and algebraic algorithms inverting equation (3) are severely behind the multistep algorithms in accuracy because they reproduce the function $< f(\mathbf{r}) >$, i.e., reconstruct the tomograms that are a priori blurred due to averaging. In fact the singlestep reconstruction helps localize an inhomogeneity, but it cannot say anything about its size and shape. In order to compensate for blurring and get useful information for the successful structure analysis and proper diagnosis in the end, the reconstructed tomograms must be subject to posprocessing.

This chapter describes two methods of postprocessing that are complementary and used successively one after another. The first implies iterative restoration with the use of the spatially variant blurring model by Nagy et al. (2004) which is described by a system of linear algebraic equations, whose matrix contains information on blurring in different regions of the image being restored. The system is inverted using iterative algorithms which solve systems with very sparse matrices. The method was developed for restoring aerospace photographs and we adapted it to diffuse optical images (Konovalov et al., 2007b) as well as to X-ray radiograms taken in X-pinch rays (Konovalov et al., 2006c). Section 2 of this chapter gives a detailed description of the method and gives examples on the restoration of model diffusion tomograms reconstructed with the PAT method. It is shown that space-varying restoration helps significantly clear the blurring and offset inhomogeneity shape distortions present on blurred tomograms. Unfortunately, the method is incapable of the accurate restoration of step functions and inhomogeneities defined by constant values of optical parameters are still reproduced with blurred boundaries. The second phase of postprocessing implies the use of nonlinear color interpretation methods (Mogilenskikh, 2000) developed at the Russian Federal Nuclear Center – Zababakhin Institute of Applied Physics for the purpose of getting more informative images of hydrodynamic plasma objects. The methods are based on the generation of nonlinear analytical and statistical functions of correspondence (hereafter correspondence function – CF) between image intensity and color space. They are described in Section 3 of this chapter. Nonlinear CFs are

applied to restored tomograms to segment and identify inhomogeneity boundaries. It is shown that in case of simple model objects (absorbing macro-inhomogeneities in a homogeneous scattering medium) it is possible to find a combination of nonlinear CFs which allows the boundaries of inhomogeneities to be reconstructed completely. Section 4 formulates basic inferences and outlines further research to improve the methods of diffusion tomogram postprocessing.

2. Space-varying restoration of diffusion tomograms

2.1 Validation of linear spatially variant blurring model

In the theory of linear systems and transforms (Papoulis, 1968) the image blurring caused by systematic errors of a visualization system is described with a model of a linear filter. Such a model is successfully used in projection tomography for estimating the accuracy of the spatial structure reproduction (Konovalov et al., 2006a; Very & Bracewell, 1979). It introduces into consideration a point spread function (PSF) that is defined as the image of an infinitesimally small point object and specifies how points in the image are distorted. A diffuse optical tomograph in general is not a linear filter because of the absence of regular rectilinear trajectories of photons. However, the PAT method that we use for reconstruction possesses a number of features which in our opinion warrant the application of a model of a linear filter in the given particular case of DOT. These features are as follows:

a. Our concept proposes the conditional PATs to be used for reconstruction as regular trajectories.
b. The PATs are close to straight lines inside the object and bend only near its boundaries.
c. The algorithms where all operations and transformations are linear are used for reconstruction.

Therefore, the PSF at the first order approximation may be assumed for describing the blurring due to reconstruction.

Let us consider at once the variance of the PSF against spatial shift. The time integral of the function $P[\mathbf{r},\tau\ (\mathbf{r}_s\ ,0) \rightarrow (\mathbf{r}_d\ ,t)]$ for each τ describes instantaneous distribution of diffuse photon trajectories. At time moment $\tau = t$ this distribution forms a zone of the most probable trajectories of photons migrated from $(\mathbf{r}_s\ ,0)$ to $(\mathbf{r}_d\ ,t)$. This zone is shaped as a banana (Lyubimov et al., 2002; Volkonskii et al., 1999) with vertices at the points of source and receiver localizations on the boundary of the scattering object. The effective width of this zone estimates the theoretical spatial resolution and is described by the standard rootmean-square deviation of photon position from the PAT as follows

$$\Delta(\tau) = \left[\int_V |\mathbf{r} - \mathbf{R}(\tau)|^2 P[\mathbf{r},\tau\,|\,(\mathbf{r}_s,0) \rightarrow (\mathbf{r}_d,t)]d^3r \right]^{1/2}, \qquad (4)$$

where $\mathbf{R}(\tau$) is a radius-vector describing the PAT. According to equation (4), as the object boundary is approached, the theoretical resolution tends to zero. In the center, the resolution is worst and depends on the object size. Thus, the resolution and, therefore, the PSF describing the PAT tomogram blurring are strongly variant against the spatial shift. It means that the spatially variant blurring model may exclusively be assumed for restoration of the PAT tomograms.

The generic spatially variant blurring would require a point source at every pixel location to fully describe the blurring operation. Since it is impossible to do this, even for small images,

some approximations should be made. There are several approaches to the restoration of images degraded by the spatially variant blurring. One of them is based on a geometrical coordinate transformation (Sawchuk, 1974) and uses coordinate distortions or known symmetries to transform the spatially variant PSF into one that is spatially invariant. After applying a spatially invariant restoration method, the inverse coordinate distortion is used to obtain the result. This approach does not satisfy us because the coordinate transformation functions need to be known explicitly. Another approach considered, for example, in (Fish et al., 1996), is based on the assumption that the blurring is approximately spatially invariant in small regions of the image domain. Each region is restored using its own spatially invariant PSF, and the results are then sewn together to obtain the restored image. This approach is laborious and also gives the blocking artifacts at the region boundaries. To restore the PAT tomograms, we use the blurring model recently developed by Nagy et. al. (2004). According to it the blurred image is partitioned into many regions with the spatially invariant PSFs. However, rather than deblurring the individual regions locally and then sewing the individual results together, this method interpolates the individual PSFs, and restores the image globally. It is clear that the accuracy of such method depends on the number of regions into which the image domain is partitioned. The partitioning where the size of one region tends to a spatial resolution seems to be sufficient for obtaining a restoration result of good quality.

2.2 Description of blurring model

Let $\mathbf{f}$ be a vector representing the unknown true image of the object function $f(\mathbf{r})$ and let $<\mathbf{f}>$ be a vector representing the reconstructed image $<f(\mathbf{r})>$ blurred due to averaging. The spatially variant blurring model of Nagy et al. (2004) is described by a system of linear algebraic equations

$$< \mathbf{f} > = \mathbf{A} \cdot \mathbf{f}, \qquad (5)$$

where $\mathbf{A}$ is a large ill-conditioned matrix that models the blurring operator (blurring matrix). If the image is partitioned into m regions, the matrix $\mathbf{A}$ has the following structure

$$\mathbf{A} = \sum_{j=1}^{m} \mathbf{D}_j \mathbf{A}_j, \qquad (6)$$

where $\mathbf{A}_j$ is a matrix that contains information on the spatially invariant PSF assigned to the j-th region of the image and $\mathbf{D}_j$ is a diagonal matrix satisfying the condition

$$\sum_{j=1}^{m} \mathbf{D}_j = \mathbf{I}, \qquad (7)$$

where $\mathbf{I}$ is the identity matrix. The piecewise constant interpolation implemented implies that the i-th diagonal entry of $\mathbf{D}_j$ is one if the i-th pixel is in the j-th region, and zero otherwise. The matrix $\mathbf{A}_j$ is uniquely determined by a single column $\mathbf{a}_j$ that contains all of the non-zero values in $\mathbf{A}_j$. This vector $\mathbf{a}_j$ is obtained from the invariant PSF $\mathbf{PSF}_j$ corresponding to the j-th region as follows

$$\mathbf{a}_j = vec(\mathbf{PSF}_j^{T}), \qquad (8)$$

where the operator $vec(\cdot)$ transforms matrices into vectors by stacking the columns.

0	0	0
0	f	0
0	0	0

f	f	f
f	f	f
f	f	f

f_{rc}	f_r	f_{rc}
f_c	f	f_c
f_{rc}	f_r	f_{rc}

Fig. 1. Standard boundary conditions: (a) zero, (b) periodic, (c) reflexive (f_c is obtained by the transposition of columns f, f_r by the transposition of rows f, f_{rc} by the transposition of rows and columns)

The blurring matrix **A** accounts for a priori information on the extrapolation of the restored image beyond its boundaries, i.e. boundary conditions. This is necessary to compensate for near-boundary artifacts caused by Gibbs effect. The blurring model implements three type of "standard" boundary conditions: zero, periodic and reflexive. The zero boundary conditions correspond to image extension by zeros (Figure 1(a)). The periodic boundary conditions assume that the image is periodically repeated (extended) in all directions (Figure 1(b)). Finally, the reflexive boundary conditions mean that the image is specularly (i.e., normally) reflected at the boundary (Figure 1(c)). The matrix $\mathbf{A}_j$ is banded block Toeplitz matrix with banded Toeplitz blocks (Kamm & Nagy, 1998) if the zero boundary conditions are used, or the banded block circulant matrix with banded circulant blocks (Andrews & Hunt, 1977) for the periodic boundary conditions, or the sum of banded block Toeplitz matrix with banded Toeplitz blocks and the banded block Hankel matrix with banded Hankel blocks (Ng et al., 1999) for the reflexive boundary conditions. The "banding" of matrix $\mathbf{A}_j$ means that the matrix-vector multiplication product $\mathbf{D}_j\mathbf{A}_j\mathbf{z}$, where $\mathbf{z}$ is any vector defined into the image domain, depends on the values of $\mathbf{z}$ in the j-th region, as well as on values in other regions within the width of the borders of the j-th region. The matrix-vector multiplication procedure is implemented by means of the 2D discrete fast Fourier transform and is fully described in (Nagy & O'Leary, 1997). Note that the standard boundary conditions may give the bandpass artifacts, if the image contains complex structures adjoining to the boundary. In this case a special approach to image extrapolation is needed (Konovalov et al., 2006c).

To simulate the invariant PSF corresponding to an individual region, first of all we must choose a characteristic point and specify a point inhomogeneity in it. It is advisable to choose the center of the region for location of the point inhomogeneity. Then we must perform two steps as follows:

a. Simulate optical projections from the point inhomogeneity.
b. Reconstruct the tomogram with PSF by the PAT method.

The optical projections from the point inhomogeneity are simulated via the numerical solution of the time-dependent diffusion equation with the use of the finite element method (FEM). To guarantee against inaccuracy of calculations, we optimize the finite element mesh so that it is strongly compressed in the vicinity of the point inhomogeneity location. For FEM calculations the point inhomogeneity is assigned by three equal values into the nodes of the little triangle on the center of the compressed vicinity. The example of the mesh for the circular scattering object 6.8 cm in diameter is given in Figure 2.
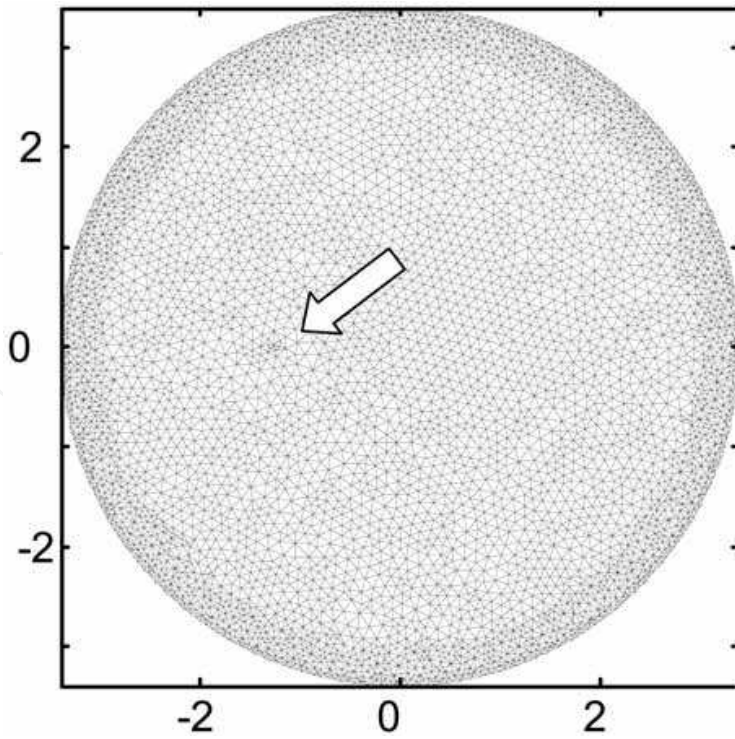
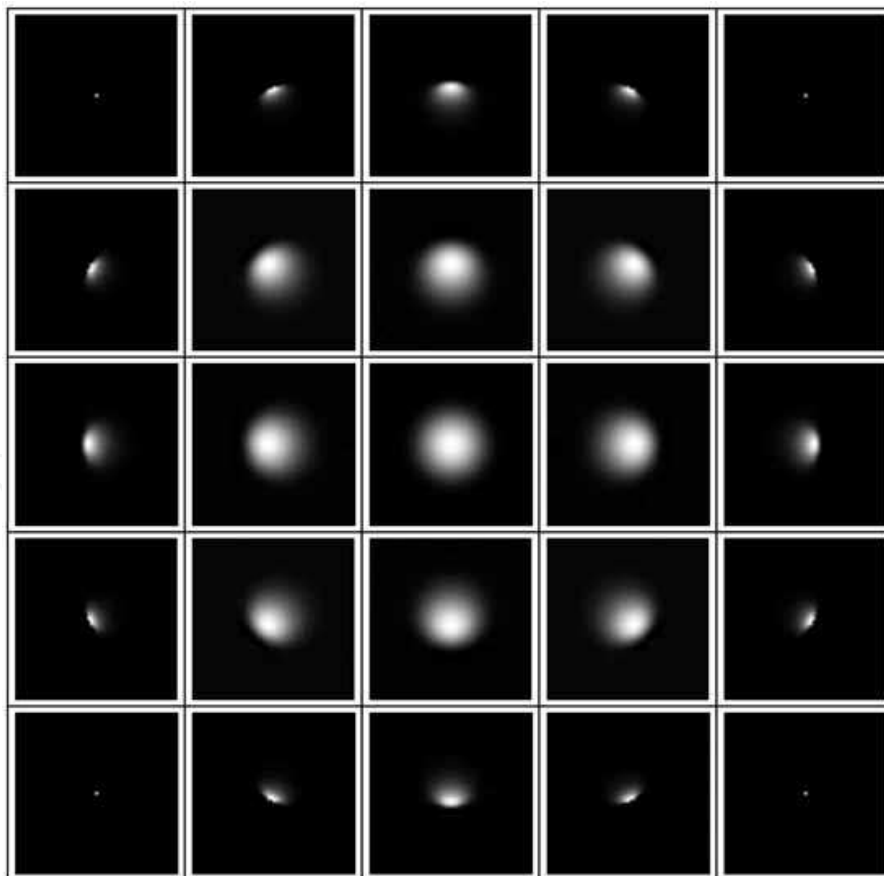Fig. 2. High-resolution finite element mesh with the compressed vicinity

Fig. 3. The 5×5 array of the invariant PSFs corresponding to individual regions of the image domain

$$
\begin{array}{ll}
\textbf{CGLS} & \textbf{MRNSD} \\[4pt]
\mathbf{f} =<\mathbf{f}> & \mathbf{f} =<\mathbf{f}> \\[4pt]
\mathbf{r} =<\mathbf{f}>-\mathbf{Af} & \mathbf{g} = \mathbf{A}^T(\mathbf{Af}-<\mathbf{f}>) \\[4pt]
\mathbf{g} = \mathbf{A}^T\mathbf{r} & \mathbf{F} = diag(\mathbf{f}) \\[4pt]
\gamma = \|\mathbf{g}\|^2 & \gamma = \mathbf{g}^T\mathbf{Fg} \\[4pt]
\text{for } k = 1,2,\ldots & \text{for } k = 1,2,\ldots \\[4pt]
\quad \text{if } k == 1, \ \mathbf{s} = \mathbf{g} & \quad \mathbf{s} = -\mathbf{Fg} \\[4pt]
\quad \text{otherwise } \mathbf{s} = \mathbf{g}+(\gamma/\gamma_{old})\mathbf{s} & \quad \mathbf{u} = \mathbf{As} \\[4pt]
\quad \mathbf{u} = \mathbf{As} & \quad \alpha = \min(\gamma/\mathbf{u}^T\mathbf{u}, \min_{s_i<0}(-f_i/s_i)) \\[4pt]
\quad \alpha = \gamma/\|\mathbf{u}\|^2 & \quad \mathbf{f} = \mathbf{f}+\alpha\mathbf{s} \\[4pt]
\quad \mathbf{f} = \mathbf{f}+\alpha\mathbf{s} & \quad \mathbf{F} = diag(\mathbf{f}) \\[4pt]
\quad \mathbf{r} = \mathbf{r}-\alpha\mathbf{u} & \quad \mathbf{z} = \mathbf{A}^T\mathbf{u} \\[4pt]
\quad \mathbf{g} = \mathbf{A}^T\mathbf{r} & \quad \mathbf{g} = \mathbf{g}+\alpha\mathbf{z} \\[4pt]
\quad \gamma_{old} = \gamma , \gamma = \|\mathbf{g}\|^2 & \quad \gamma = \mathbf{g}^T\mathbf{Fg} \\[4pt]
\text{end} & \text{end}
\end{array}
$$

Fig. 4. The step sequences describing the restoration algorithms

Figure 3 presents the array of the invariant PSFs calculated for the case of image partitioning into 5×5 regions.

2.3 Restoration algorithms

After constructing the blurring matrix $\mathbf{A}$, an acceptable algorithm should be chosen to solve system (5) for unknown vector $\mathbf{x}$. Because of the large dimensions of the linear system, iterative algorithms are typically used to compute approximations of $\mathbf{f}$. They include a variety of least-squares algorithms (Bjorck, 1996), the steepest descent algorithms (Kaufman, 1993), the expectation-maximization algorithms (Bertero & Boccacci, 1998), and many others. Since non of the iterative algorithm is optimal for all image restoration problems, the study of iterative algorithms is an important area of research. In present paper we consider the conjugate gradient algorithm CGLS (Bjorck, 1996) and the steepest descent algorithm MRNSD (Kaufman, 1993). These algorithms represent two different approaches: a Krylov subspace method applied to the normal equations and a simple descent scheme with enforcing a nonnegativity constraint on solution. The step sequences describing the algorithms are given in Figure 4. The operator $\|\cdot\|$ denotes a Euclidian norm, the function $diag(\cdot)$ produces the diagonal matrix containing the initial vector.

Both CGLS and MRNSD are easy to implement and converge faster than, for example, the expectation-maximization algorithms. Both the algorithms exhibit a semi-convergence behavior with respect to the relative error $\|\mathbf{f}_k - \mathbf{f}\|/\|\mathbf{f}\|$, where $\mathbf{f}_k$ is the approximation of $\mathbf{f}$ at the k-th iteration. It means that, as the iterative process goes on, the relative error begins to decrease and, after some optimal iteration, begins to rise. By stopping the iteration when the error is low, we obtain a good regularized approximation of the solution. Thus, the iteration

number plays the role of the regularization parameter. This is very important for us, as the matrix **A** is severely ill-conditioned and regularization must be necessarily incorporated. To estimate the optimal iteration number, we use the following blurring residual that measures the image quality change after beginning the restoration process:

$$\beta_k = \|\mathbf{f}_k - \mathbf{f}\| / \|< \mathbf{f} > -\mathbf{f}\| \% . \tag{9}$$

Like the relative error, the blurring residual has a minimum that corresponds to the optimal iteration number. Note that we do not know the true image (vector **f**) in clinical applications of DOT. However, using criterion $\beta_k \to$ min , it is possible to calibrate the algorithms in relation to the optimal iteration number via experiments (including numerical experiments) with phantoms. In general many different practical cases of optical inhomogeneities can be considered for calibration. In clinical explorations, the particular case is chosen from a priori information, which the blurred tomograms contain after reconstruction. Further, regularization can be enforced in a variety of other ways, including Tikhonov (Groetsch, 1984), iteration truncation (Hanson & O'Leary, 1993), as well as mixed approaches. Preconditioned iterative regularization by truncating the iterations is an effective approach to accelerate the rate of convergence (Nagy et al., 2004). In general, preconditioning amounts to finding a nonsingular matrix **C** , such that $\mathbf{C} \approx \mathbf{A}$ and such that **C** can be easily inverted. The iterative method is then applied to preconditioned system

$$\mathbf{C}^{-1} < \mathbf{f} > = \mathbf{C}^{-1}\mathbf{A} \cdot \mathbf{f} . \tag{10}$$

The appearance of matrix **C** is defined by the regularization parameter $\lambda < 1$ that characterizes a step size at each iteration. In this paper we consider two methods for calculating λ: generalized cross validation (GCV) method (Hanson & O'Leary, 1993) and method based on criterion of blurring residual minimum. In the first case we assume that a solution computed on a reduced set of data points should give a good estimate of missing points. The GCV method finds a function of λ that measures the errors in these estimates. The minimum of this GCV function corresponds to the optimal regularization parameter. In the second case we calculate blurring residual (9) for different numbers of iterations and different discrete values of λ, taken with the step $\Delta\lambda$. The minimum of blurring residual corresponds to optimal number of iterations and the optimal regularization parameter.

The main reason of choosing MRNSD for PAT tomogram restoration is that this algorithm enforces a nonnegativity constraint on the solution approximation at each iteration. Such enforcing produces much more accurate approximate solutions in many practical cases of nonnegative true image (Kaufman, 1993). In DOT (for example, optical mammotomography), when the tumor structure is detected, one can expect that the disturbances of optical parameters are not randomly inhomogeneous functions, but they are smooth or step nonnegative ones standing out against a close-to-zero background and forming the macroinhomogeneity images. Indeed, the typical values of the absorption coefficient are between 0.04 and 0.07 cm^{-1} for healthy breast tissue, and between 0.07 and 0.1 cm^{-1} for breast tumor (Yates et al., 2005). Thus, we have the nonnegative true image f (**r**). This a priori information gives the right to apply constrained MRNSD and change negative values for zeros after applying unconstrained CGLS.

2.4 Restoration results

To demonstrate the effect of blurring reduction on PAT-reconstructed tomograms, a numerical experiment was conducted, wherein circular and rectangular scattering objects with absorbing inhomogeneities were reconstructed from model optical projections and then restored. In this chapter we present processing results for five objects whose description and parameters are given in Table 1. To simulate the optical projections, we solved the timedependent diffusion equation with the instantaneous point source for photon density by the FEM. The signals of the receivers were found as photon fluxes on the object boundary. Each optical projection was calculated as logarithm of the non-perturbed signal determined for the homogeneous medium to the signal perturbed due to inhomogeneities. For all objects from Table 1 we used the measurement ratio 32×32 (32 sources and 32 receivers). The circular objects were reconstructed by the backprojection algorithm with convolution filtering (Konovalov et al., 2003; 2007b; Lyubimov et al., 2003) and the rectangular ones with the modified multiplicative algebraic reconstruction technique (Konovalov et al., 2006b; 2007a). To restore the reconstructed tomograms, in all cases we partitioned the image domain into 5×5 regions and applied the reflexive boundary conditions.
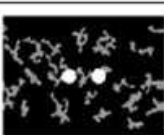
Description	Visual model	Sizes, cm	Optical parameters			
			f^{obj} cm^{-1}	f^{inh} cm^{-1}	D cm	n
Circular object with 1 cm-in-diam inhomogeneity		Ø6.8	0.05	0.075	0.066	1.4
Circular object with two 1 cm-in-diam inhomogeneities						
Circular object with two 1.4 cm-in-diam inhomogeneities						
Rectangular object with two 1 cm-in-diam inhomogeneities		11×8			0.034	
Rectangular object with two 1 cm-in-diam inhomogeneities and RIC				0.075 (inhom) 0.06 (RIC)		

Table 1. Description and parameters of the model scattering objects: f^{obj}, absorption coefficient of the object; f^{inh}, absorption coefficient of the inhomogeneities; D, diffusion coefficient; n, refraction index; RIC, randomly inhomogeneous component

Figure 5 shows results of restoration for the circular object with the inhomogeneity 1 cm inndiameter in comparison with its blurred tomogram. The results are presented as gray level images. The axes are graduated in centimeters and the palette scale is in inverse centimeters. The points on the images present the positions of the sources on the boundary

of the object. The circle on the left image shows the true boundary of the inhomogeneity. It is seen that restoration allows getting closer to its actual size.
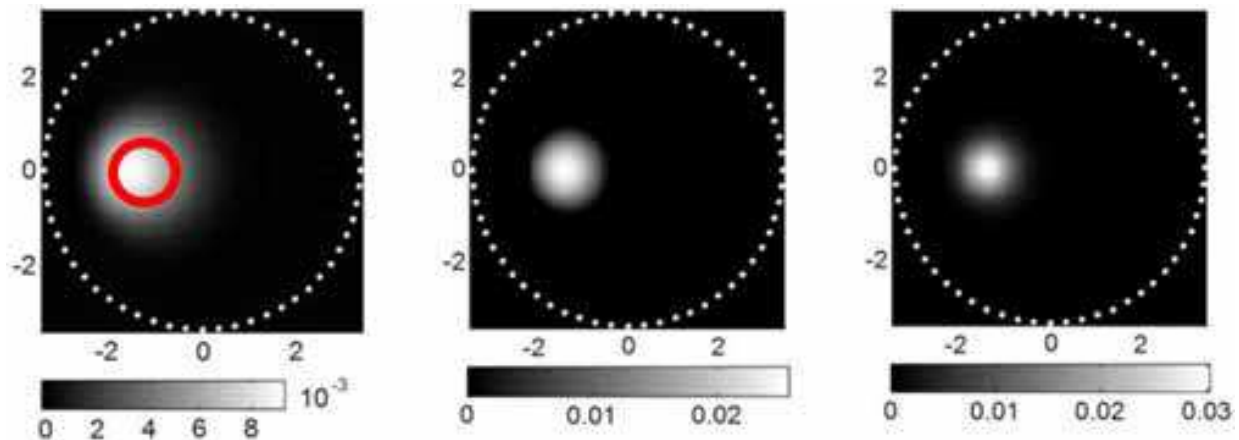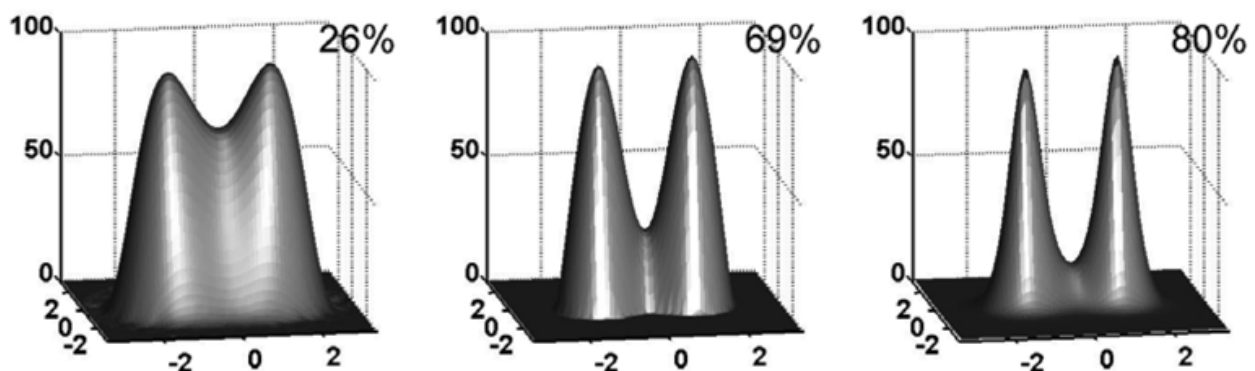

Fig. 5. Reconstruction and restoration results for the circular object with the inhomogeneity 1 cm in diameter: blurred tomogram (left) and results of its restoration by CGLS and MRNSD (center and right)

Figure 6 shows pseudo-3D plots representing the same results for the circular object with two inhomogeneities that form a periodic structure. Digits on the plots show the values of the modulation transfer coefficient estimated as the relative depth of the dish between two peaks. This figure demonstrates that restoration helps significantly increase the modulation transfer coefficient and hence the spatial resolution of tomograms. For all restorations presented in Figures 5 and 6 we used the unpreconditioned algorithms (CGLS and MRNSD). The optimal iteration number obtained by the criterion of blurring residual minimum is equal to 15 in the case of CGLS and to 9 in the case of MRNSD, respectively.

Fig. 6. Reconstruction and restoration results for the circular object with two inhomogeneities 1 cm in diameter: blurred tomogram (left) and results of its restoration by CGLS and MRNSD (center and right)

Figure 7 presents the restoration results obtained with the use of preconditioned MRNSD. The left image corresponds to the regularization parameter calculated by the GCV method ($\lambda = 0.003$). To obtain the central restoration, we used preconditioner with $\lambda = 0.1$. This value of the regularization parameter was found by the criterion of blurring residual minimum. The right image in Figure 7 shows the result of restoration by unpreconditioned MRNSD for comparison. The optimal iteration number in the cases of preconditioned algorithm was

equal to 3. Thus, preconditioners allow the restoration procedure to be accelerated. But, as it follows from Figure 7, preconditioned algorithms distort the form of inhomogeneities being restored. We can conjecture that the image partitioning into 5×5 regions is not enough to obtain good quality of restoration by preconditioned algorithms. As we save computational time, in future the image partitioning number may be increased.
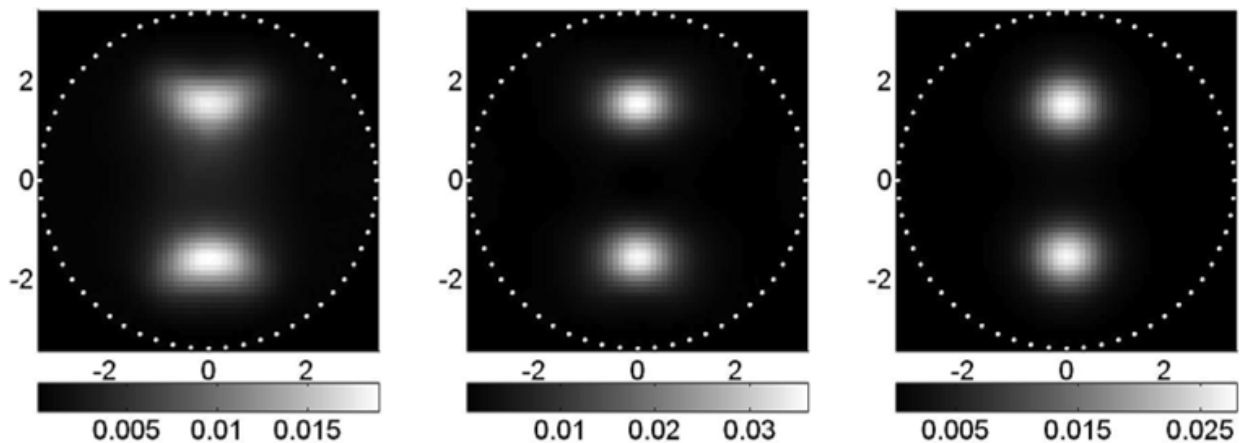

Fig. 7. Comparison of the restoration results obtained with the use of preconditioned MRNSD (left and center) and unpreconditioned one (right) for the circular object with two inhomogeneities 1.4 cm in diameter

Figure 8 demonstrates results obtained in the testing of unpreconditioned MRNSD for noise immunity. The left image shows the 20%-noised sinogram that is a gray level map of optical projection distributions over the index ranges of the source and the receiver. The sinogram abscissa is the receiver index and the sinogram ordinate is the source index. The palette scale is graduated in relative units. Despite the fact that the reconstructed tomogram (center) is strongly blurred, the restored image (right) has only low distortion in the shape of inhomogeneities. Thus, the restoration algorithm demonstrates good immunity to measurement noise.
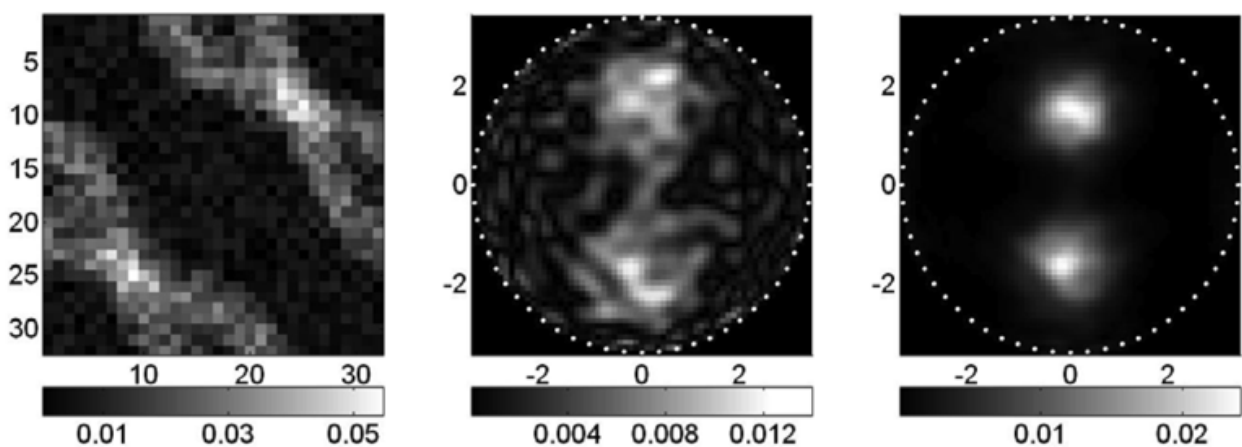

Fig. 8. 20%-noised sinogram (left), blurred tomogram (center) and restoration with unpreconditioned MRNSD (right) for the circular object with two inhomogeneities 1.4 cm in diameter

Figure 9 compares the spatially variant model by Nagy and a spatially invariant model that is described by one PSF defined in the center of the tomogram domain. In the latter case the

centers of inhomogeneities are seen to be abnormally shifted from their true positions marked with crosses.
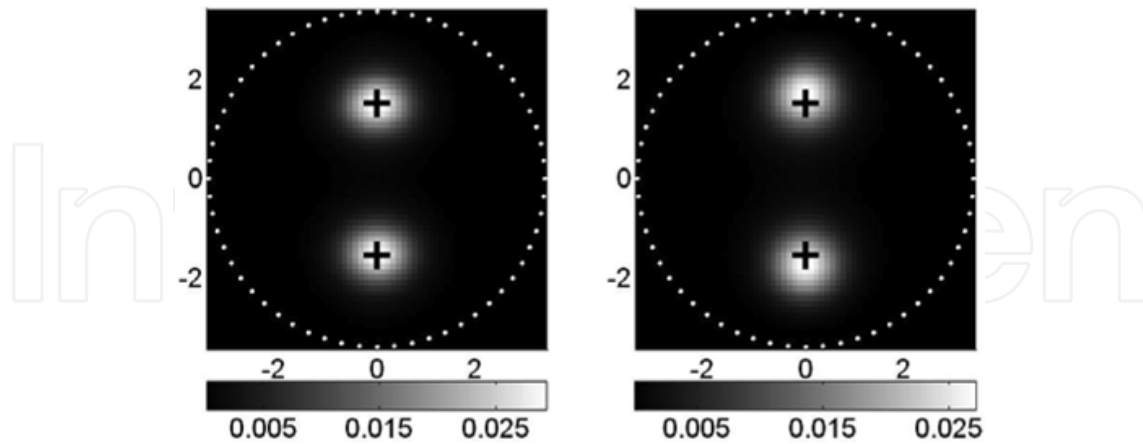

Fig. 9. Restoration results for the circular object with two inhomogeneities 1.4 cm in diameter, obtained with spatially variant (left) and spatially invariant (right) blurring models

Finally Figure 10 presents reconstruction and restoration results for the rectangular object with two inhomogeneities 1 cm in diameter (and without RIC). Here unpreconditioned MRNSD was applied.
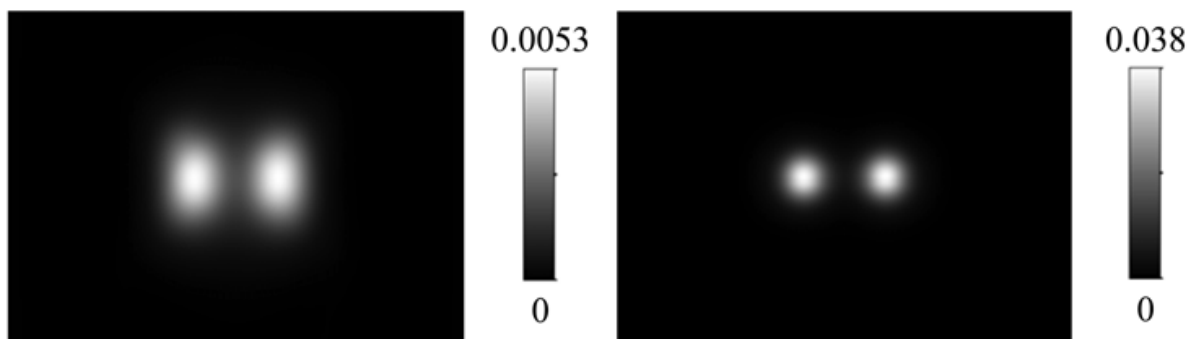

Fig. 10. Reconstruction and restoration results for the rectangular object with two inhomogeneities 1 cm in diameter: blurred tomogram (left) and the result of its MRNSD restoration (right)

The results presented thus confirm that blurring of PAT tomograms can be reduced through iterative restoration. The spatially variant model helps adequately estimate the actual size of inhomogeneities, but as follows, for instance, from Figure 6, further processing is needed to reconstruct inhomogeneity boundaries and get reliable information on its shape because even after restoration inhomogeneity profiles have a "gaussian" form, being far from the ideal steps typical of true images.

3. Segmentation with nonlinear CFs

3.1 CF generation algorithms
To segment restored diffusion tomograms, i.e. to reconstruct the boundary and shape of optical inhomogeneities, we use nonlinear color interpretation methods (Konovalov et al., 2007; Mogilenskikh, 2000) based on the generation of nonlinear analytical and statistical

functions of correspondence between image intensities (values of the restored object function) and palette colors. A palette is an ordered set of colors from color space where each color is assigned a number. If the pallet is linear, then the set of its colors create a straight trajectory in color space. The curvilinear trajectory corresponds to the nonlinear palette.

The analytical CFs imply the use of nonlinear color coordinate scales for attaining correspondence between intensity and color in a cell. Elementary functions and their algebraic combinations are used for this purpose. What particular combination is taken depends on the operator and a priori information contained in restored tomograms.

The nonlinear statistical CFs are generated using statistical information on the distribution of colors of an initially chosen palette (as a rule, linear) over image cells. The algorithm we have implemented can be described in brief by the following steps.

a. A linear CF is generated, i.e. a color $G\,(f_{kl})$ from the linear palette chosen is assigned to image intensity f_{kl} in a cell with indexes k and l.

b. The number of cells $N_G^{cells}\,(f_{kl})$ of each color from the palette is calculated; then a weight vector, whose size is equal to the number of colors in the palette, is calculated as

$$W_G(f_{kl}) = N_{col}\,\mathrm{norm}\!\left[\frac{N_G^{cells}(f_{kl})+1}{N^{cells}}\right], \tag{11}$$

where N_{col} is the number of colors in the palette, N^{cells} is the total number of cells in the image and norm($\cdot$) is a normalization operator.

c. The statistical CF is calculated from the collected statistics as a spline. We use the following simple spline:

$$G^{stat}(f_{kl}) = \left[G(f_{kl}) - N_{col}\,\mathrm{norm}(f_{kl})\right]\cdot\left[W_G(f_{kl}) - W_{G+1}(f_{kl})\right] + W_G(f_{kl}). \tag{12}$$

d. The nonlinear CF is generated by summing the statistical CF (12) and the initial linear CF.

Our experience (Konovalov et al., 2007) suggests that combinations of nonlinear analytical and statistical CFs give best results in the context of the segmentation problem solution. Indeed, the use of the statistical CF is needed to ultimately get a step palette. And before that it is advisable to "focus" the boundary of the inhomogeneity, which is clearly "gaussian" after space-varying restoration, by applying a nonlinear smooth function. Also inhomogeneity images after restoration exhibit a large percentage of background (zero or almost zero) values and before applying the statistical CF it is advisable to somewhat "level" statistics with respect to background values and inhomogeneity intensities.

Note that such a segmentation method based on the generation of nonlinear CFs compares favorably with the standard threshold filtration where some part of the image is rejected and replaced by a background value of the object function which may result in the loss of important details in the reproduction of randomly inhomogeneous structures. Nonlinear CFs are applied to all pixels in the image and if their parameters are well chosen, we manage not to lose, but effectively segment the informative details of the image.

3.2 Examples of nonlinear CF application to restored tomograms

For the analytical CF we tried power and exponential functions and found the latter to be more effective. An exponential function written as $G(f) = \exp(B_1 f) + B_2$ was parametrized so

that the coefficients B_1 and B_2 were determined from the equality of volumes of the figures bounded by the object function $f(x, y)$ before and after image transformation that consisted in the successive application of the analytical and statistical CFs. The statistical CF was automatically generated with the algorithms described in Section 3.1. For the purpose of parametrization we had to state and solve the problem of minimizing the difference between figure volumes. Since image transformation on the whole does not have the analytical representation, the optimal parameters were found with a simple direct search algorithm (Lagarias et al., 1998) that does not require the numerical or analytic calculation of gradients.
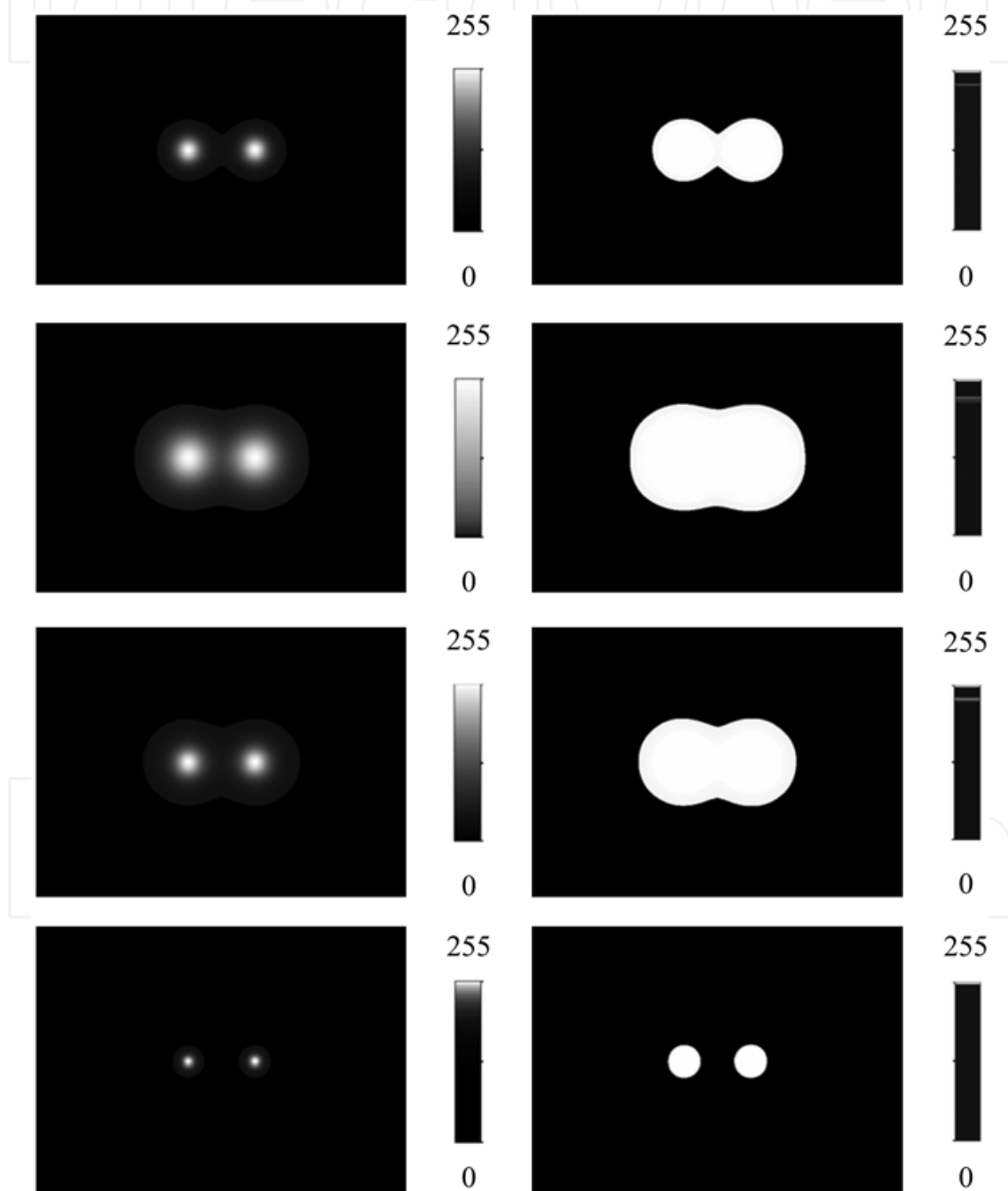
Fig. 11. Examples of nonlinear CF application to the restored tomogram of the rectangular object with two inhomogeneities 1.0 cm in diameter

Figure 11 illustrates examples of nonlinear CF application to the restored tomogram of the rectangular object with two inhomogeneities 1.0 cm in diameter (see the right image of Figure 10). The left column of images shows the effects of the analytical CFs (top down): the power function $G(f) = f_2$, the power function $G(f) = f$, the exponential function $G(f) = \exp(f)$ and the parametrized exponential function $G(f) = \exp(B_1 f) + B_2$. The right column demonstrates what was obtained after applying statistical CFs. Image intensities are normalized. It follows from Figure 11 that for "simple" models (absorbing macro-inhomogeneities in a homogeneous scattering medium), it is possible to obtain such a combination of nonlinear CFs that allows the true structure of inhomogeneities to be reconstructed almost completely. Indeed, if apply subtraction to the lowest right image of Figure 11 and the normalized true image of the inhomogeneities, we obtain the three-tone pattern shown in Figure 12 (coincidence is in grey and difference is in black and white).
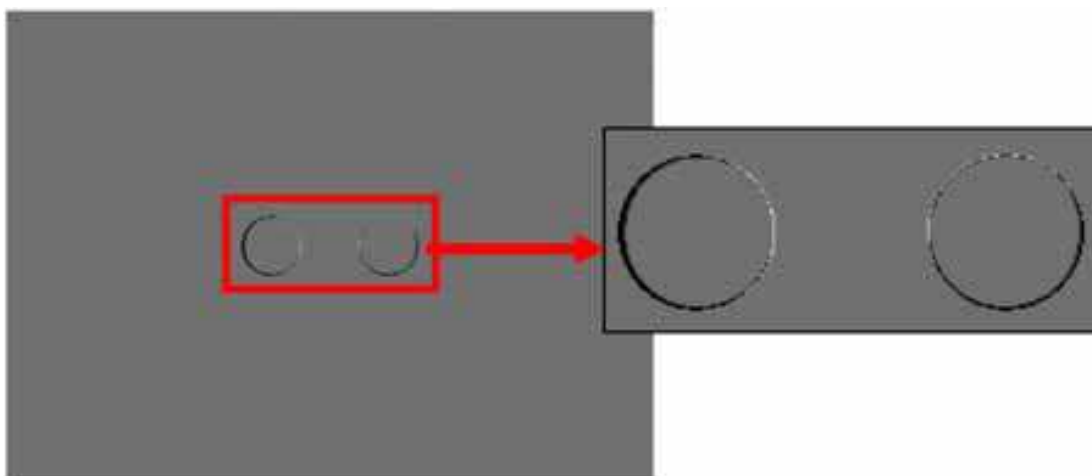
Fig. 12. The three-tone pattern characterizing how the result of postprocessing agrees with the true image

Figure 13 shows an object defined on a finite element mesh, which models a randomly inhomogeneous medium with macro-inhomogeneities and Figure 14 demonstrates results of its reconstruction (upper left), restoration (upper right) and nonlinear postprocessing (lower left and right).
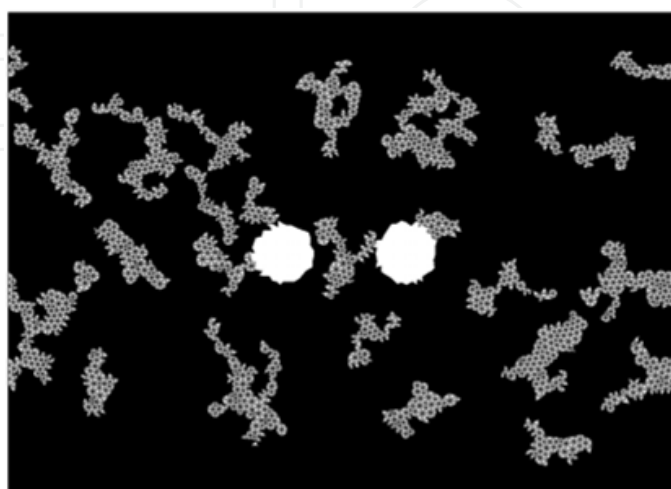

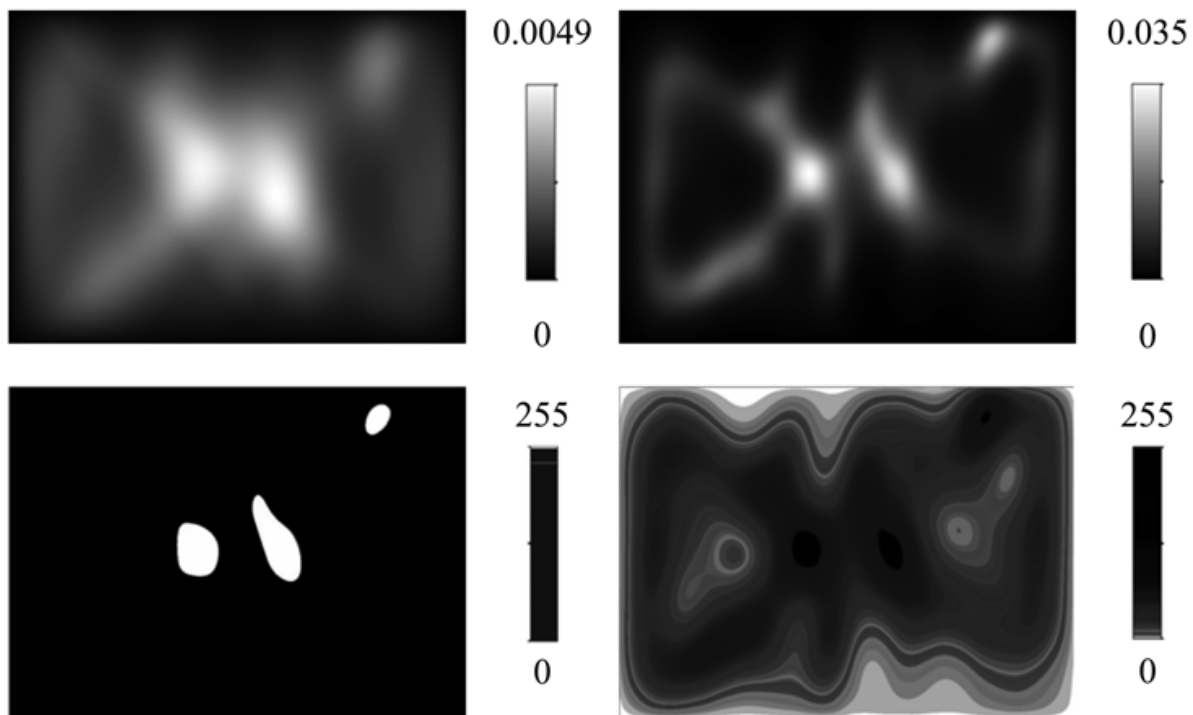Fig. 13. The rectangular object with two inhomogeneities 1.0 cm in diameter and RIC

Fig. 14. Reconstruction and postprocessing results for the object of Figure 13

The lower left image resulted from the successive application of the parametrized exponential and statistical CFs to the restored tomogram and the lower right image was obtained after applying the statistical CF without preprocessing with analytical functions. It is seen that our segmentation method in the case of the complex model of Figure 13 give inhomogeneity shape distortions and artifacts (the upper structure on the lower left image) which may however be removed on the basis of a priori information contained in restored tomograms. The lower right image demonstrates an attempt to segment inhomogeneities with no use of analytical CFs. One must admit that the visual examination of reproduced results in this case is much more inconvenient.

In conclusion we should note that the two-step postprocessing of one image on Intel PC with the 1.7-GHz Pentium 4 processor and 256-MB RAM in MATLAB takes less than 30 seconds. The reconstruction of blurred tomograms takes to 5 seconds if integral algorithms are applied and to 30 seconds if iterative algebraic ones are used. The total time is thus below 1 minute. The comparative analysis of computational speed presented in (Lyubimov et al., 2002) suggests that the use of the well-known package TOAST (Temporal Optical Absorption and Scattering Tomography, Schweiger & Arridge, 2008) which implements the Newton-Raphson algorithm will make the time of restoration several times longer. It should also be noted that there are good prospects for making the postprocessing procedure yet faster by using not MATLAB, but a faster programming environment and optimizing the measurement ratio. Our investigation (Konovalov et al., 2007a) suggests that the number of sources can be reduced from 32 to 16 almost with no loss in reproduction quality.

4. Conclusion

In this chapter we have demonstrated the effective application of two-step postprocessing to the diffuse optical tomograms restored from model optical projections with the photon

average trajectory method. The first step involves iterative restoration with the spatially variant blurring model and the second is segmentation with nonlinear palettes and nonlinear functions of correspondence between image intensities and palette colors. The first step helps reduce blurring due to averaging over the spatial distribution of diffuse photons and get information on the actual size of reproduced inhomogeneities. The boundary and shape of inhomogeneities are segmented at the second step. It is shown that the true image can almost completely be reconstructed for simple model objects (circular absorbing macro-inhomogeneities in a homogeneous scattering medium). For complex models of randomly inhomogeneous media, the proposed method of postprocessing may give distortions and artifacts. Therefore of certain interest is further investigation into methods that would help optimize the algorithms of correspondence function generation and obtain images without artifacts.

5. Acknowledgments

6. References

Andrews, H. & Hunt, B. (1977). *Digital Image Restoration*, Prentice-Hall, Englewood Cliffs, New York.

Arridge, S. R. (1999). Optical tomography in medical imaging. *Inverse Problems*, Vol. 15, No. 2, April 1999, pp. R41–R93.

Bertero, M. & Boccacci, P. (1998). *Introduction to Inverse Problem in Imaging*, IOP, London.

Bjorck, A. (1996). Numerical Methods for Least Square Problems, SIAM, Philadelphia.

Boas, D. A.; Brooks D. N.; Miller, E. L.; DiMarzio, C. A.; Kilmer, M.; Gaudette, R. J. & Zhang, Q. (2001). Imaging the body with diffuse optical tomography. *IEEE Signal Processing Magazine*, Vol. 18, No. 6, November 2001, pp. 57-75.

Fish, D. A.; Grochmalicki, J. E. & Pike, R. (1996). Scanning singular-value-decomposition method for restoration of images with space-variant blur. *Journal of the Optical Society of America A: Optics, Image Science & Vision*, Vol. 13, No. 3, March 1996, pp. 464-469.

Gibson, A. P.; Hebden, J. C. & Arridge, S. R. (2005). Recent advances in diffuse optical imaging. *Physics in Medicine & Biology*, Vol. 50, No. 4, February 2005, pp. R1–R43.

Groetsch, C. W. (1984). The Theory of Tikhonov Regularization for Fredholm Integral Equations of the First Kind, Pitman, Boston.

Hanson, P. C. & O'Leary, D. P. (1993). The use of the L-curve in the regularization of discrete ill-posed problems. *SIAM Journal on Scientific Computing*, Vol. 14, No. 6, November 1993, pp. 1487–1503.

Herman, G. T. (1980). Image Reconstruction from Projections: The Fundamentals of Computerized Tomography, Academic, New York.

Kak, A. C. & Slaney, M. (1988). *Principles of Computerized Tomographic Imaging*, IEEE Press, New York.

Kalintsev, A. G.; Kalintseva, N. A.; Kravtsenyuk, O. V. & Lyubimov, V. V. (2005). Superresolution in diffuse optical tomography. *Optics & Spectroscopy*, Vol. 99, No. 1, July 2005, pp. 152–157.

Kamm, J. & Nagy, J. G. (1998). Kronecker product and SVD approximation in image restoration. *Linear Algebra & Its Applications,* Vol. 284, No. 1-3, November 1998, pp. 177-192.

Kaufman, L. (1993). Maximum likelihood, least squares, and penalized least squares for PET. *IEEE Transactions on Medical Imaging,* Vol. 12, No. 2, February 1993, pp. 200–214.

Konovalov, A. B.; Kiselev, A. N. & Vlasov V. V. (2006a). Spatial resolution of few-view computed tomography using algebraic reconstruction techniques. *Pattern Recognition & Image Analysis,* Vol. 16, No. 2, April 2006, pp. 249-255.

Konovalov, A. B.; Lyubimov, V. V.; Kutuzov, I. I.; Kravtsenyuk, O. V.; Murzin, A. G.; Mordvinov, G. B.; Soms, L. N. & Yavorskaya, L. M. (2003). Application of the transform algorithms to high-resolution image reconstruction in optical diffusion tomography of strongly scattering media. *Journal of Electronic Imaging,* Vol. 12, No. 4, October 2003, pp. 602-612.

Konovalov, A. B.; Mogilenskikh, D. V.; Vlasov, V. V. & Kiselev, A. N. (2007a). Algebraic reconstruction and post-processing in incomplete data computed tomography: from X-rays to laser beams, In: *Vision Systems: Applications*, Obinata, G. & Dutta, A. (Eds.), Chapter 26, pp. 487-518, I-Tech Education and Publishing, Vienna.

Konovalov, A. B.; Vlasov, V. V.; Kalintsev, A. G.; Kravtsenyuk, O. V. & Lyubimov, V. V. (2006b). Time-domain diffuse optical tomography using analytic statistical characteristics of photon trajectories. *Quantum Electronics*, Vol. 36, No. 11, November 2006, pp. 1048-1055.

Konovalov, A. B.; Vlasov, V. V.; Kravtsenyuk, O. V. & Lyubimov, V. V. (2007b). Spacevarying iterative restoration of diffuse optical tomograms reconstructed by the photon average trajectories method. *EURASIP Journal on Advances in Signal Processing*, Vol. 2007, No. 3, March 2007, ID 34747.

Konovalov, A. B.; Vlasov, V. V.; Uglov, A. S.; Shelkovenko, T. A. & Pikuz, S. A. (2006c). Iterative restoration of X-ray images taken in X-pinch rays. *Proceedings of the 2nd International Symposium on Communications, Control and Signal Processing (ISCCSP'2006),* on CD-ROM, Marrakech, March 2006, Suvisoft Oy Ltd. publisher, Tampere.

Kravtsenyuk, O. V. & Lyubimov, V. V. (2000). Application of the method of smooth perturbations to the solution of problems of optical tomography of strongly scattering objects containing absorbing macroinhomogeneities. *Optics & Spectroscopy*, Vol. 89, No. 1, July 2000, pp. 107–112.

Lagarias, J. C.; Reeds, J. A.; Wright, M. H. & Wright, P. E. (1998). Convergence properties of the Nelder-Mead simplex method in low dimensions. *SIAM Journal on Optimization*, Vol. 9, No. 1, January 1998 pp. 112-147, 1998.

Lyubimov, V. V.; Kalintsev, A. G.; Konovalov, A. B.; Lyamtsev, O. V.; Kravtsenyuk, O. V.; Murzin, A. G.; Golubkina, O. V.; Mordvinov, G. B.; Soms L. N. & Yavorskaya L. M. (2002). Application of photon average trajectories method to real-time reconstruction of tissue inhomogeneities in diffuse optical tomography of strongly scattering media. *Physics in Medicine & Biology,* Vol. 47, No. 12, June 2002, pp. 2109-2128.

Lyubimov, V. V.; Kravtsenyuk, O. V.; Kalintsev, A. G.; Murzin, A. G.; Soms, L. N.; Konovalov, A. B.; Kutuzov, I. I.; Golubkina O. V. & Yavorskaya, L. M. . (2003). The

possibility of increasing the spatial resolution in diffusion optical tomography. *Journal of Optical Technology*, Vol. 70, No. 10, October 2003, pp. 715–720.

Mogilenskikh, D. V. (2000). Nonlinear color interpretation of physical processes, *Proceedings of the 10th International Conference on Computer Graphics and Vision (GRAPHICON'2000)*, pp. 201-211, Moscow, August-September 2000, Moscow State University publisher, Moscow.

Nagy, J. G. & O'Leary, D. P. (1997) Fast iterative image restoration with a spatiallyvarying PSF, In: *Advanced Signal Processing: Algorithms, Architectures, and Implementations VII*, Luk, F. T. (Ed.), *Proceedings of SPIE*, Vol. 3162, pp. 388-399, SPIE, Bellingham.

Nagy, J. G.; Palmer, K. & Perrone, L. (2004). Iterative methods for image deblurring: a Matlab object oriented approach. *Numerical Algorithms*, Vol. 36, No. 1, May 2004, pp. 73–93.

Ng, M. K.; Chan, R. H. & Tang, W.-C. (1999). A fast algorithm for deblurring models with Neumann boundary conditions. *SIAM Journal on Scientific Computing*, Vol. 21, No. 3, November-December 1999, pp. 851–866.

Papoulis, A. (1968). Systems and Transforms with Applications in Optics, McGraw-Hill, New York.

Sawchuk, A. A. (1974). Space-variant image restoration by coordinate transformations. *Journal of the Optical Society of America*, Vol. 64, No. 2, February 1974, pp. 138–144.

Schweiger, M. & Arridge, S. R. (2008). http://web4.cs.ucl.ac.uk/research/vis/toast.

Very, J. G. & Bracewell, R. N. (1979). Blurring in tomograms made with X-ray beams of finite width. *Journal of Computer Assisted Tomography*, Vol. 3, No. 5, May 1979, pp. 662–678.

Volkonskii, V. B.; Kravtsenyuk, O. V.; Lyubimov, V. V.; Mironov, E. P. & Murzin, A. G. (1999). The use of the statistical characteristics of the photons trajectories for the tomographic studies of the optical macroheterogeneities in strongly scattering objects. *Optics & Spectroscopy*, Vol. 86, No. 2, February 1999, pp. 253–260.

Webb, S. (1998). *The Physics of Medical Imaging*, Institute of Physics Publishing, Bristol.

Yates, T.; Hebden, J. C.; Gibson, A.; Everdell, N.; Arridge, S. R. & Douek, M. (2005). Optical tomography of the breast using a multi-channel time-resolved imager. *Physics in Medicine & Biology*, Vol. 50, No. 11, June 2005, pp. 2503-2517.

Yodh, A. & Chance, B. (1995). Spectroscopy and imaging with diffusing light. *Physics Today*, Vol. 48, No. 3, March 1995, pp. 34–40.

Computer Vision

Edited by Xiong Zhihui

This book presents research trends on computer vision, especially on application of robotics, and on advanced approachs for computer vision (such as omnidirectional vision). Among them, research on RFID technology integrating stereo vision to localize an indoor mobile robot is included in this book. Besides, this book includes many research on omnidirectional vision, and the combination of omnidirectional vision with robotics. This book features representative work on the computer vision, and it puts more focus on robotics vision and omnidirectioal vision. The intended audience is anyone who wishes to become familiar with the latest research work on computer vision, especially its applications on robots. The contents of this book allow the reader to know more technical aspects and applications of computer vision. Researchers and instructors will benefit from this book.

INTECH
open science | open minds